VII International Conference on Textile Composites and Inflatable Structures
STRUCTURAL MEMBRANES 2015
E. Oñate, K.-U.Bletzinger and B. Kröplin (Eds)

NUMERICAL ANALYSIS OF AN ELASTO-FLEXIBLE WING CONFIGURATION USING COMPUTATIONAL FLUID STRUCTURAL SIMULATIONS

J. PIQUEE[*] AND C. BREITSAMTER[†]

[*] Institute of Aerodynamics and Fluid Mechanics,
Technische Universität München,
85748 Garching, Germany
e-mail: julie.piquee@aer.mw.tum.de, web page: https://www.aer.mw.tum.de

[†] Institute of Aerodynamics and Fluid Mechanics,
Technische Universität München,
85748 Garching, Germany
e-mail: christian.breitsamter@aer.mw.tum.de, web page: https://www.aer.mw.tum.de

Key words: Elasto-flexible wing, Coupled RANS and FEM Simulations, Coupled Panel method and analytical membrane code, SST model, γ-Re_θ transition model

Summary: In the present work, different numerical approaches dealing with fluid and structural interaction models are introduced to simulate the aerodynamics and structural behavior of 2D elasto-flexible wings. In order to verify the models, the results are compared with the experimental data based on wind tunnel investigations conducted at the Institute of Aerodynamics and Fluid Mechanics of the Technische Universität München. The results show a good agreement while the findings are to some extent similar to sailwing configurations: the lift is higher than on the rigid counterpart geometry whereas the drag is nearly equivalent and the stall region is smoother and appears delayed.

1 INTRODUCTION

With an average growth rate of nearly 30% each year over the past five years[1], energy produced by wind has been the fastest growing source of energy in the world today. With global warming and rising fuel prices, the wind energy industry will still significantly play an important role in the future. However, it still remains important to improve the technology in order to keep economically wind energy competitive.

Increasing the rotor diameter and therefore the turbine size could offer a more efficient way to produce energy with wind turbines: a larger turbine can indeed capture more energy throughout its lifetime. However larger turbines means higher structural and fatigue loads[2], which can cause more possible damages and then more unscheduled maintenance. The control of loads of a turbine has then led to intensive research in order to keep the wind energy domain competitive. Among others Basualdo[3] numerically investigated a rear-mounted flap concerning

its impact on loads. The study was conducted using a potential theory method for a variable-geometry airfoil by analyzing the changes in the airfoil displacements. The displacements affect directly the fatigue of the material through the bending moment. It was found that the use of a flapped airfoil can lead to load alleviation by reducing the airfoil displacement variations. Therefore, a variable geometry airfoil appears as a possible solution for the wind energy domain to increase performance. Such a design also suggests an alleviation of the effects of gust winds, which can result in a reduction of loads and fatigues.

For Micro Air Vehicles, an increasing amount of resources has already been spent to investigate vehicles able to alter their shape like wings featuring a flexible membrane, with the main goal of improving their efficiency and reducing loads[4,5,6]. The aerodynamic force measurements show that aerodynamics characteristics of elasto-flexible membrane airfoils/wings are comparable or even better than their rigid counterparts[7,8]. Due to the flexibility of the airfoil/wing, its shape can adapt itself to the free stream flow by changing its geometry, which will induce new aerodynamics and structural properties. This adaptation to the flow results also in a delayed stall region: it was experimentally shown that flexible membrane airfoils/wings stall at higher angle of attack. For example, typical rigid wing for Micro Air Vehicles have stall angles between 12° and 15°, whereas flexible wings, which reduce their effective angle of attack to the surface deformation, may have stall angles up to 30° and 45°[5].

This paper focuses on a 2D elasto-flexible airfoil and has the purpose to present a numerical investigation of such a configuration. The numerical work was made by developing a coupling between fluid and structure solvers in order to simulate the strong relation between the mechanical and aerodynamic properties. The paper will present two different models to simulate the behavior of the 2D elasto-flexible airfoil: on one hand a Panel-method code coupled with an analytical membrane description and on the other hand a CFD-U/RANS simulation coupled with a FEM program at low Reynolds number ($0.23\text{x}10^6$).

2 MODEL GEOMETRY AND NUMERICAL METHODS

The geometry used in this work, which is illustrated in Fig. 1, has been developed within an experimental study[9]: the corresponding investigation considers an elasto-flexible membrane wrapped around rigid leading- and trailing-edge spars. The leading-edge spar is made of a double ellipse to reduce the gradient of pressure which facilitates flow separation[9,10], whereas the trailing-edge spar was designed as a sharp element for 2D experiments. The membrane material used for the wing surface was chosen for its compliance to adapt itself to the flow free stream and for its resistance as it has to be strong enough to bear the aerodynamic loads. In the experiments[9], the membrane is a highly extensible, anisotropic elastic fabric coat covered with an impermeable rubber layer. As the membrane is an anisotropic material, its mechanical properties are dependent on all the directions and are linked with each other: the nonlinear deformation of the membrane depends on the ratio of the applied loads in the warp and in the weft directions[11]. However, for some reasons of simplicity, it was decided to consider the material as an isotropic material for both numerical models with a Young modulus equal as the Young modulus in the weft direction with $E=2.1MPa$. The pre-stress of the membrane was also

taken into account as it controls significantly the deformation of the membrane: the initial elongation of the membrane is equal to 2% in the chord direction[9].

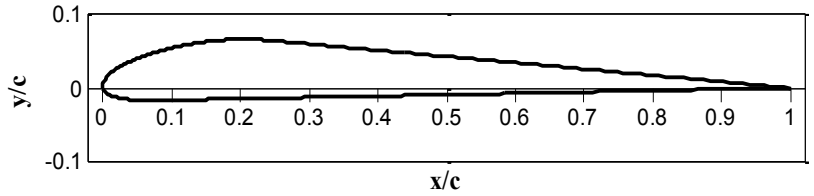

Figure 1 – Geometry of the elasto-flexible wing configuration

2.1 Panel method coupled with an analytical membrane model

The first method to simulate such a configuration was realized with the software Matlab by developing a Panel method code coupled with an analytical membrane model. Based on a discretization of the body, this method consists on finding the pressure distribution around the geometry divided into panels and then determining the deformation of the elasto-flexible membrane defined within the analytical membrane behavior.

As the Panel method is a well-known method, a detailed description of the model will not be given here, but for more information the reference[12] can be used. Nevertheless, a brief description of the membrane code will be given; for more details, the references[10,13] can be used. The membrane code is based on the theoretical membrane deflection equation which is for a 2D case described by Eq. (1)

$$t_x \frac{\partial^2 z(x)}{\partial x^2} = -(P(x) - P_\infty), \tag{1}$$

where the parameter *z(x)* represents the deflection of the membrane at the position (x), $P(x) - P_\infty$ the pressure difference at the position (x) and t_x the tension component defined as:

$$t_x = t_{xo} + K_x \Delta l_x. \tag{2}$$

The parameter K_x is defined as material property and Δl_x is the elongation of the membrane in the x-direction. Eq. (1) represents the relationship between the curvature of the membrane, the tension and the difference of pressure which will induce the deformation. The membrane is considered to be fixed at the leading-edge ($x = 0$) and at the trailing-edge ($x = c$). The introduction of the point x_s, defined as the point where the membrane will separate from the contour of the leading-edge spar, is then important to find the new shape of the airfoil. Therefore, between $x = 0$ and $x \leq x_s$, the airfoil geometry is given by the leading-edge geometry, whereas for $x > x_s$, the shape is determined by the deflection of the membrane which is given by solving Eq. (1). The boundary conditions of Eq. (1) are given in the following:

$$z(x_s) = z_L(x_s) \tag{3}$$

$$z'(x_s) = z_L{}'(x_s) \tag{4}$$
$$z(c) = 0. \tag{5}$$

Eq. (3) assures that the membrane contour is the same as the leading-edge contour up to station *xs*, then Eq. (4) assures that the separation between the membrane and the leading-edge will appear smoothly and finally Eq. (5) illustrates the fixing condition of the membrane at the trailing-edge. The solution of Eq. (1) is obtained by integrating Eq.(1) two times as it is shown by Eq. (6), obtaining an equation for the parameter x_s:

$$z(x) = \frac{1}{t_x}\int_{xs}^{x}\int_{xs}^{x}\Delta P(x).dx.dx \; + \; \frac{dz_L(x)}{dx}_{x_s}.x + (z_L(x_s) - \frac{dz_L(x)}{dx}_{x_s}.x_s), \tag{6}$$

$$\text{with} \quad t_x = \frac{\int_{xs}^{c}\int_{xs}^{c}\Delta P(x).dx.dx}{(c-x_s).\frac{dz_L(x)}{dx}_{x_s} + z_L(x_s)}. \tag{7}$$

To entirely solve the system, x_s needs to be found: the method is to express the elongation of the membrane in two different ways. The point x_s where those expressions are equal (Eq. (8)) will give the final solution.

$$\frac{l(x_s)-l_o}{l_o} = \frac{t_x}{E_m} - \varepsilon_o, \tag{8}$$

with l_o as initial length of the membrane, E_m the Young Modulus of the membrane and ε_o the initial pre-elongation.

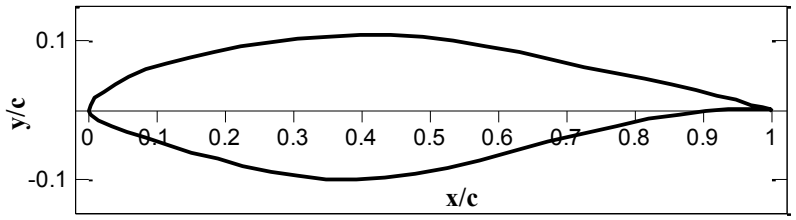

Figure 2 – S812 Airfoil Geometry

In order to validate the Panel code developed with Matlab, it was decided to compare the pressure distribution along the airfoil S812 (Fig. 2) and the lift coefficient for different angles of attack with those obtained with the software Xfoil and with experimental data[15]. At an angle of attack of $\alpha=2°$, different numbers of panels were tested (Tab. 1) to check the influence of the discretization on the results. Fig. 3 shows the evolution of the lift coefficient obtained at $\alpha=2°$ for different numbers of panels which vary from 200 to 5000 around the S812 profile. As it is expected, the lift coefficient value increases with the number of panels up to a certain value. In this case, the final value of the lift coefficient obtained at $\alpha=2°$ with 5000 panels is equal to 0.6028. The software Xfoil provides 0.6025 with 400 panels and within the experiment a lift

coefficient of 0.49 at a Reynolds number of 10^6 is obtained. Considering Xfoil as a reference, the error of the Panel code is then 0.05%. In Figs. 4 and 5 the pressure distribution is plotted for the S812 profile at 2° obtained with the Panel method for 200, 500 and 2000 panels as well as with Xfoil and by the experiments. The pressure distribution along the profile is well-approximated with the Panel method when it is compared with the distribution obtained with Xfoil. Nevertheless, a difference is noticeable at the trailing edge, where a reverse pressure and a peak can be observed with the Panel method code. However the reverse pressure disappears whereas the peak augments when the number of panels increases. These unphysical phenomena is caused by the interpolation of the profile which is based on a cubic spline interpolation between the given grid points of the profile. Considering the experimental data, the Panel code overestimates the pressure along the profile which explains the difference between the lift coefficient values at $\alpha=2°$, presented in Tab. 1.

For the following, it was decided to work with 2000 panels as the error (compared with Xfoil) obtained at $\alpha=2°$ for the S812 profile is already below 0.5%. The lift coefficient from $\alpha=-2°$ to $8°$ for the S812 profile obtained with Xfoil and the Panel code is listed in Tab. 1. The relative error remains below 3%.

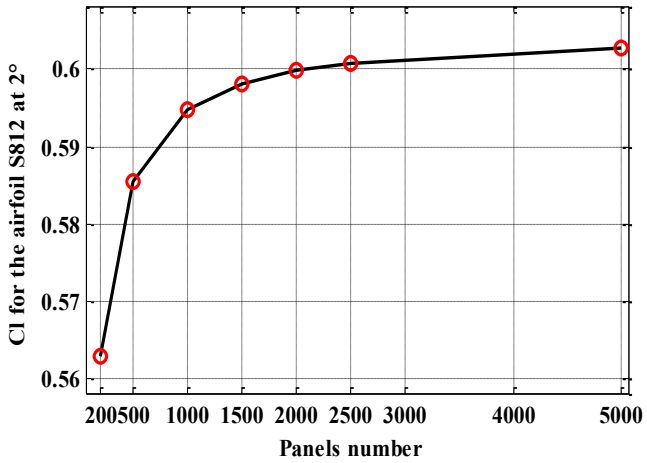

Figure 3 – Evolution of the lift coefficient with the number of panels

Table 1 – Lift coefficient comparison between the Panel Method code and Xfoil for different angles of attack

α/Lift Coeffi-cient	Panel Method α=2°	Xfoil	Error (%)	Experim-ental Data
0°	0.350	0.353	0.91	0.26
2°	0.6	0.603	0.45	0.49
4°	0.849	0.851	0.26	0.71
6°	1.097	1.098	0.13	0.94
8°	1.343	1.344	0.04	1.03

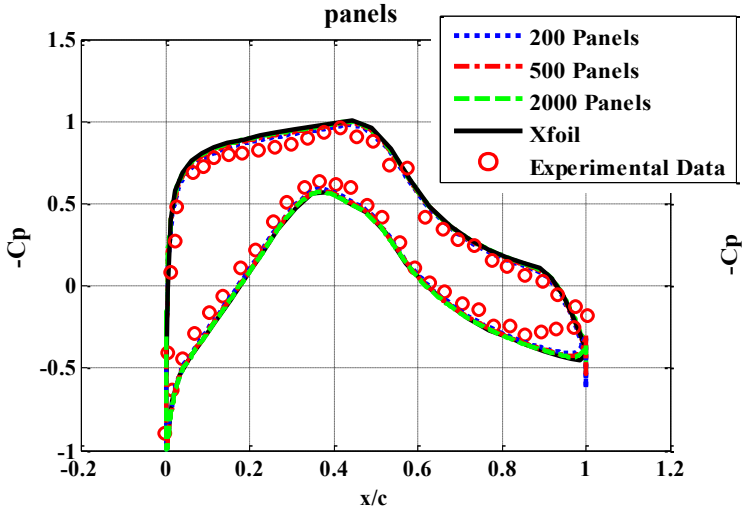

Figure 5 – Pressure coefficient distribution at 2° for the S812 profile

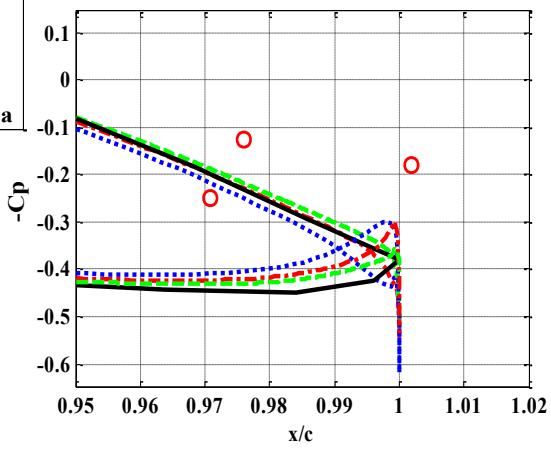

Figure 4 – Pressure coefficient distribution at 2° for the S812 profile

2.2 Fluid structure simulations performed with CFD ans FEM

The second method concentrates on Fluid-Structure-Interaction simulations based on a coupling between the fluid solver ANSYS CFX (CFD-U/RANS method) and the structural solver STATIC STRUCTURAL (FEM method), directly controlled by the Workbench of ANSYS. As the structural deformations of the airfoil are significant to change the fluid flow itself, the so called 2-ways interaction simulations were performed using a mesh motion inside the fluid solver. The displacement of the mesh is controlled by a mesh stiffness parameter, which controls which regions deform to absorb the motion and which remain relatively rigid. The mesh motion is applied near the small volumes as the deformation of the fluid grid appears inside the boundary layer of the airfoil, which is composed of the thinnest nodes.

- **Fluid model**

The fluid solver software used in this work is ANSYS CFX. As the considered Reynolds number is small, namely $\mathrm{Re} = 0.23\mathrm{x}10^6$, according to the Mayle correlation[14], the percentage of laminar flow relative to the chord length is estimated to be more than 5%. As the laminar-turbulent transition phenomenon affects the pressure distribution, the deformation and the behavior of the elasto-flexible wing, two models concerning the fluid simulations were investigated within ANSYS CFX: the k-ω based SST turbulence model and the k-ω based SST coupled with the transition γ-Re_θ model. Furthermore, as the Mach number is low ($Ma < 0.3$) the fluid is considered as incompressible and it is also supposed isothermal. The residual criteria are set in order that the maximal value of all the residuals should be lower than 10^{-4}. A second order upwind scheme for the convection terms is used and all the diffusion terms are discretized with the second order central difference scheme.

- **Mesh generation and Grid resolution study**

Considering the 2D airfoil geometry, a C-Grid block method is used to create a structured mesh for the fluid domain with the software Icemcfd. The C-Grid is created by using a 10/20 chord size, which means that upstream of the leading-edge, the fluid size is around 10 times the chord length and downstream of the trailing-edge, the fluid domain has the size of 20 times the chord length. An O-Grid is also created around the profile to refine the boundary layer. A value of $y^+ = 1$ is used which corresponds to a distance of the first nodes of 0.05 mm from the profile.

To avoid mesh issues dependency, a grid sensitivity study was performed. Four meshes are tested to better understand the influence of the mesh on the results and to find a suitable grid for the simulations. The non-dimensional wall distance y^+ remained constant for all grids but the number of layers inside the boundary layer and in the circumferencial direction of the body are refined with a ratio of 1.5 in both directions. The different characteristics of the grids are described in Table 2, and Figs. 6 and 7 represent the coarse and the extra-fine meshes.

Table 3 – Characteristics of the four different grids

Parameters	Coarse	Medium	Fine	Extra-fine
Total Nodes Number	74750	141210	461030	690730
Normal layer	80	120	180	270
Circumferential layer	90	140	210	345
Minimal Angle	25.5	28.8	28.8	28.3
Aspect Ratio	1266	1865	1005	633

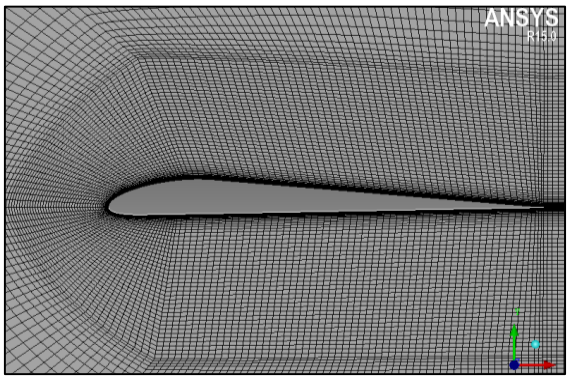

Figure 6 – Coarse Mesh

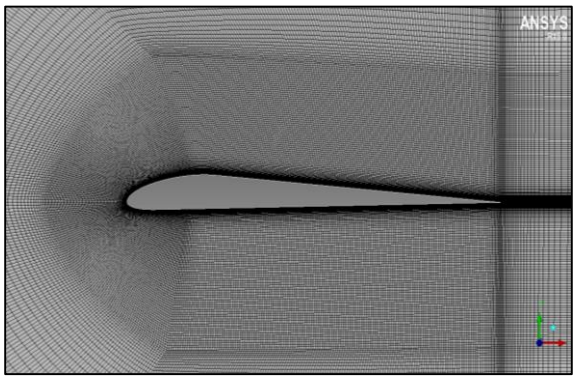

Figure 7 – Extra-fine Mesh

2.3 Experimental analysis

The experiments focusing on force measurements have been conducted in a Göttingen type wind tunnel with an elasto-flexible 2D wing model. The 2D model consists of an extension of the geometry described in Fig. 1 in the third direction set up on a support as it can be seen in Fig. 8. The model has an overall span of 564 mm and a nominal chord of 220 mm, giving an aspect ratio of AR = ~ 2.5. In order to limit 3D flow effects, end-plates of circular planform are used to reproduce two-dimensional flow condition. These end-plates have a diameter of three times the airfoil chord and are made of Plexiglas to provide an optical access to the elasto-flexible airfoil. The force measurements were conducted for an initial elongation of ΔL_o = 2% at a Reynolds number of Re = 278750.

Figure 8 – Elasto-flexible 2D model mounted in wind tunnel test section

3 RESULTS & DISCUSSION

3.1 Grid dependency

The results of the grid sensitivity study for *α=0°, 4°, 8°, 10°* and *14°* are given in Fig. 9, where the lift coefficient is plotted for the four different meshes. The numbers 1, 2, 3 and 4 of the abscissae axes correspond to the different meshes from the coarse to the extra-fine. For both models, the coarse and medium meshes overestimate or underestimate the lift coefficient for all angles of attack by sometimes 1.16% compared to the results obtained with fine and extra-fine meshes. For the SST turbulence model, the lift coefficient converges for *α=2°, 4°, 10°* and *14°* with the fine mesh: the fine mesh appears fine enough to achieve a grid independency in the results. For the γ-Re_θ transition model, the lift coefficient converges for the angles of attack *α=4°, 8°* and *14°*. For *α=0°* and *10°* there is a difference in the results between the fine and extra-fine meshes, which does not exceed 0.57%. Therefore, it was decided to perform the FSI simulations with the extra-fine mesh, which appears fine enough that there is not noticeable influence in the results.

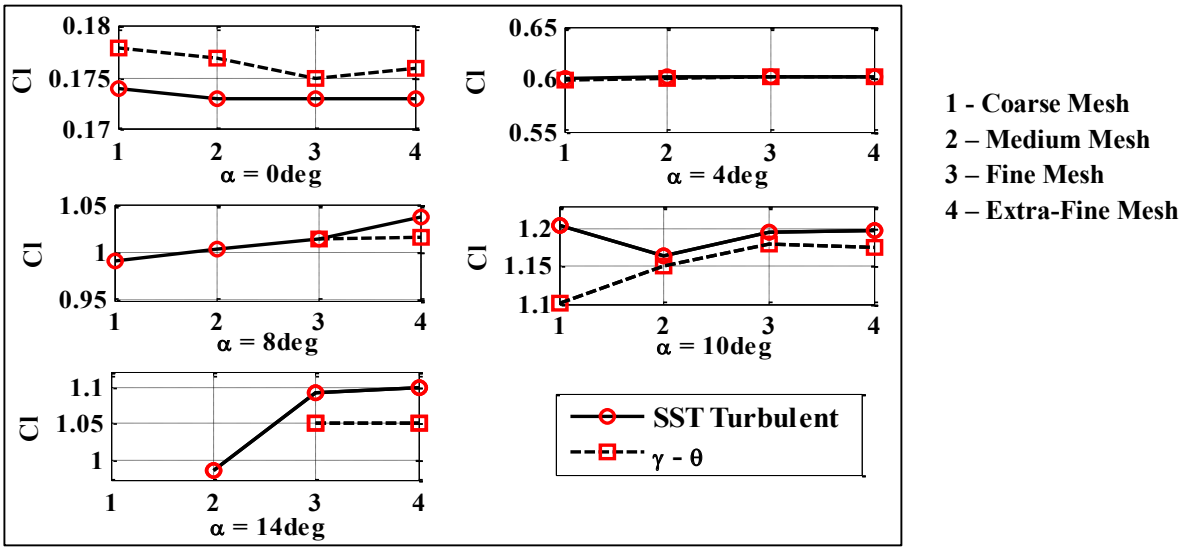

Figure 9 – Grid sensitivity study for the SST model the γ-Re_θ model for the angles of attack of *α=0°, 4°, 8°, 10°* and *14°*

3.2 γ-Re_θ Transition model

The results with the γ-Re_θ transition model are presented in Fig. 10, where the lift and drag coefficients are plotted as function of the angle of attack. In Fig. 10, the results for the Panel method, the experimental data[9] and the rigid counterpart of the elasto-flexible concept are also plotted.

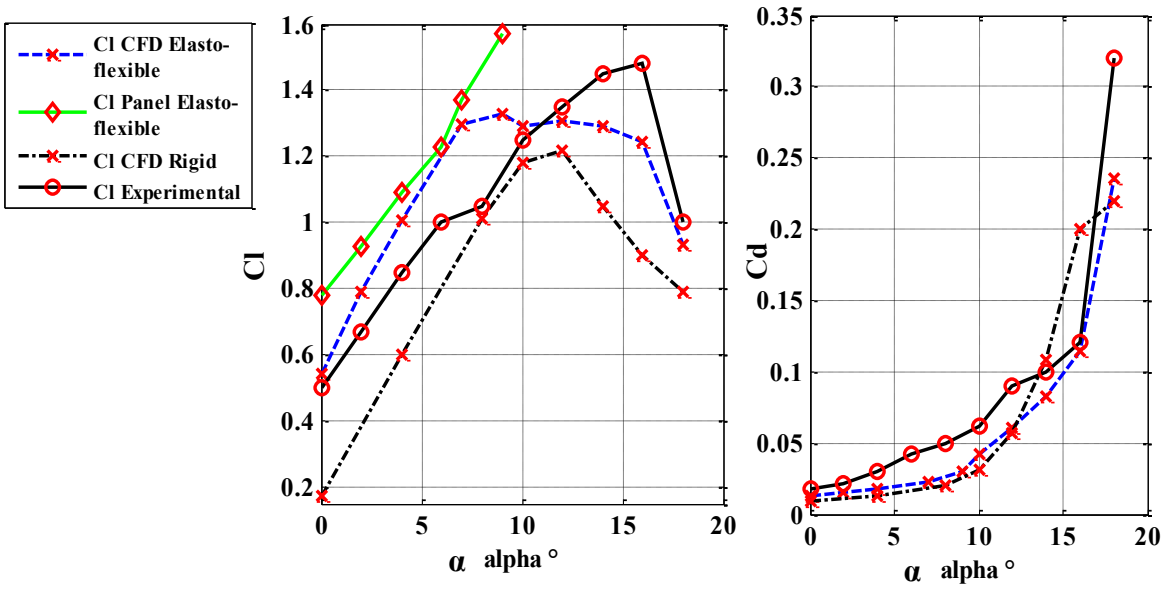

Figure 10 – Lift and Drag coefficients as function of the angle of attack for the γ-Re$_\theta$ model

The results show that the lift coefficient of an elasto-flexible wing is much higher than the lift obtained for its rigid counterpart whereas the drag coefficients are nearly equivalent. As the elasto-flexible wing can adapt itself to the flow environment, the pressure distribution along the wing causes a positive deformation of the membrane for positive angles of attack which results in an augmentation of the curvature of the profile and therefore an increase in the lift coefficient. At $\alpha=0°$ the lift coefficient of the elasto-flexible wing is about three times higher than the lift coefficient of the rigid wing (0.544/0.175) due to the curvature of the elasto-flexible wing. The lift coefficient then linearly increases until $\alpha=7°$ where the lift reaches a maximum of 1.33; from $\alpha=7°$ to $\alpha=16°$ the lift coefficient of the elasto-flexible wing stays constant which is a characteristic feature of the adaptivity of such a concept. The stall phenomenon appears over a larger angle of attack range compared to a rigid wing resulting in a smoother and delayed stall region. The elasto-flexible wing lift coefficient drops at $\alpha=16°$ whereas the lift for its rigid counterpart drops at $\alpha=12°$. In this case, Figs. 11 and 12 illustrate the turbulence intensity of the flow at $\alpha=7°$ and $\alpha=9°$. At $\alpha=7°$, a laminar separation bubble can be seen on the upper side of the profile at around 2/3 of the chord, whereas at $\alpha=9°$, the laminar separation bubble migrates to the leading-edge of the profile. Therefore, the detachment of the turbulent boundary layer appears sooner at $\alpha=9°$ compared to $\alpha=7°$. The pressure distribution at $\alpha=9°$ for the region of the turbulent boundary layer separation point up to the end of the profile is then constant and exhibits a reduced suction level compared to the pressure distribution at $\alpha=7°$; this explains the decrease of the deformation of the upper-sided membrane and therefore the small decrease of the lift coefficient. From $\alpha=9°$ to $\alpha=16°$, the point where the boundary layer detaches, moves to the leading-edge resulting in a slight and slow decrease of the deformation of the membrane (due to the constant pressure): therefore the stall phenomenon appears smooth until the boundary layer detaches at the leading-edge causing the loss of lift beyond $\alpha=16°$.

As the Panel theory does not consider the viscosity phenomena, the pressure distribution

along the profile is overestimated: the lift coefficient of the profile obtained with the Panel method is therefore also overestimated compared to the results obtained with ANSYS as it can be observed in Fig. 10.

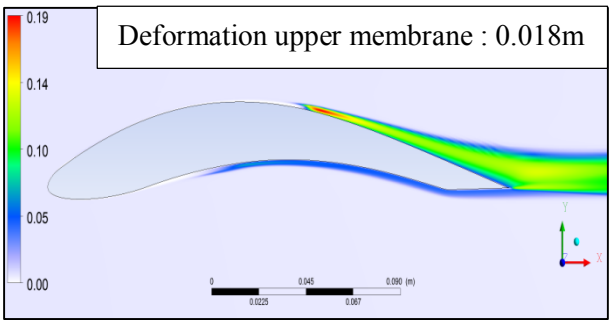

Figure 11 – Turbulence intensity for α=7°

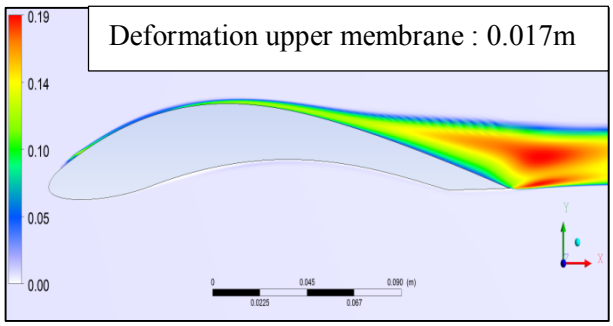

Figure 12 – Turbulence intensity for α=9°

Furthermore, it was expected that the CFD results for the lift coefficient would have been higher than the values obtained during the experiments due to the 3D-effects of the flow, which are not completely suppressed by the end plates. This is the case up to α=9°; however beyond α=9°, as it was mentioned before, the laminar separation bubble moves to the leading-edge and the turbulent boundary layer starts detaching at the trailing-edge causing a small decrease/stagnation in the lift coefficient. As the lift increases further for α>9° in the experiments, it is assumed that this phenomenon was different for the flow conditions of the wind tunnel. Nevertheless, as the force measurements were the only research topic, more investigations are necessary to conclude on the evolution of the lift during the experiment.

3.3 Fully Turbulent

The results obtained for the SST simulations are presented in Fig. 13. The lift coefficient of the elasto-flexible wing is again higher than its rigid counterpart due to the increase of the camber of the geometry. The stall region is also smoother for the elasto-flexible wing due to the slow decrease of the deformation of the upper side of the membrane. Finally, the lift coefficient is also overestimated in the Panel method as the viscosity of the flow is not taken into account.

Nevertheless, the results obtained with the SST simulations seem to fit better the experimental data compared to the results obtained with the γ-Re_θ model. Although, the lift coefficient is higher and the drag coefficient values are lower for the simulations due to the 3D-effects occurring in the experiments, for angles of attack lower than α=12°, the SST model fits better the experimental results, which supposes that the flow was completely turbulent during the experiments. The main difference between the two flow models is that the fully turbulent case does not take into account the laminar-turbulent transition. Therefore, there is no laminar separation bubble in this model and the deformation on the upper side of the membrane is smaller compared to the care obtained with the γ-Re_θ model: the lift increases continuously up to α=12° and is smaller than the lift coefficient obtained with γ-Re_θ. However, beyond α=12°, in both models the lift coefficient values are equivalent as the laminar separation bubble

migrates to the leading-edge. Then, the lift coefficient stays quite constant as the separation of the turbulent boundary layer migrates to the leading-edge up to $\alpha=16°$ where the lift drops abruptly due to the complete turbulent boundary layer separation. As the evolution of the lift appears in both fluid models different, a detailed experimental flow analysis should be undertaken to conclude on this difference.

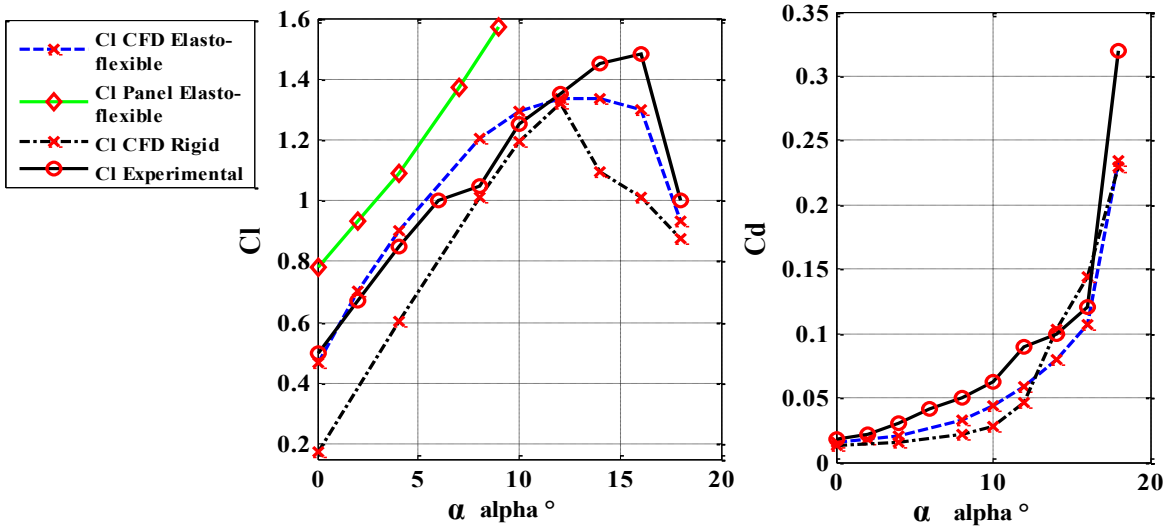

Figure 13 - Lift and Drag coefficients as function of the angle of attack for the fully turbulent model

4 CONCLUSIONS

This paper considered different numerical investigations of a 2D elasto-flexible wing at a Reynolds number of 0.23×10^6. The simulations were undertaken using two different methods: a first coupling was made between a Panel method and an analytical membrane model and a second coupling was made between U-RANS (CFX) and Finite Element Method (Static Structural) softwares within the Workbench of ANSYS. As the Reynolds number suggested that the transition could have an important role, both a fully turbulent computation with the SST turbulence model and a simulation including the γ-Re_θ transition model have been carried out.

The results show that the elasto-flexible wing provides much higher lift compared to a rigid wing of equal planform whereas the drag is nearly equivalent. Due to its adaptivity, an elasto-flexible wing has a more cambered profile compared to its rigid counterpart, which explains the aerodynamic differences between the two geometries. Furthermore, the adaptivity will permit a slow migration of the turbulent boundary layer separation to the leading-edge causing a smoother and delayed stall region. The simulations show also that the Panel method, as it was expected, overestimate the lift of such a design as it does not considere the viscosity of the flow. Moreover, due to the 3D-effects of the flow during the experiments, the simulations overestimate the experimental values obtained for the lift coefficient whereas they underestimate the drag values in the angle-of-attack range of $\alpha=9°$-$12°$. Beyond $\alpha=9°$-$12°$, the lift during the experiment increase further whereas during the simulations the lift starts stagnating: an additional flow study (pressure distribution, transition detection) should be

undertaken to better understand this difference in the results.

Finally, the main difference between SST and γ-Re_θ models occurs between α=2°-12° where a laminar separation bubble migrates from the trailing-edge to the leading-edge in the transitional fluid model. The transition model offers then a profile which provides more lift because of its more cambered geometry, as the pressure on the upper side of the membrane is higher due to the laminar boundary layer. For α=10°, both fluid models, SST and γ-Re_θ show equivalent values for the lift coefficient of the elasto-flexible wing. The results of the SST turbulent simulations fit then better the experimental values below α=10° compared to the transition model. Nevertheless, as there are big differences between experiments and simulations between α=10° and 16°, detailed experimental studies should be undertaken to conclude on the main parameters influencing the flow separation scenario.

REFERENCES

[1] Global Wind Energy Council, "Global Wind Report Annual market update 2014", online at http://www.gwec.net/wp-ontent/uploads/2015/03/GWEC_Global_Wind_2014_Report_LR.pdf.
[2] Berg, D., Johnson, S. J., and Case van Dam, C. P., "Active Load Control Techniques for Wind Turbines", Sandia Report 2008.
[3] Basulado, S., "Load alleviation on wind turbine blades using variable airfoil geometry", *Wind Engineering,* Volume 29, No. 2, 2005, pp. 169-182.
[4] Hu, H., Tamai, M., and Murohy, T., "Flexible-Membrane Airfoils at Low Reynolds Numbers", *Journal of Aircraft,* Volume 45, No. 5, September-October 2008, pp. 1767-1777.
[5] Lian, Y., and Shyy, W., "Numerical Simulations of Membrane Wing Aerodynamics for Micro Air Vehicle Applications", *Journal of Aircraft,* Volume 42, No. 4, July-August 2005, pp. 865-873.
[6] Tang., J., Viieru, D., and Shyy, W., "A Study of Aerodynamics of Low Reynolds Number Flexible Airfoils", *37th AIAA Fluid Dynamics Conference and Exhibit,* Miami, 25-28 June 2007.
[7] Fink, M., "Full-Scale Investigation of the Aerodynamic Characteristics of a Sailwing of Aspect Ratio 5.9", NASA TN D-5047, 1969.
[8] Maughmer, M. D., "A Comparison of the Aerodynamic Characteristics of Eight Sailwing Airfoils Sections", Princeton Univ. TR, 1979.
[9] Beguin, B., "Development and Analysis of an Elasto-flexible Morphing Wing Configuration", Dissertation, Technische Universität München, 2014.
[10] Murai, H., and Maruyama, S., "Theoretical Investigation of Sailwing Airfoils Taking Account of Elasticities", *Journal of Aircraft,* Volume 19, No. 5, May 1982, pp. 385-389
[11] Uhlemann, J., Stranghoener, N., Schmidt, H., and Saxe, K., "Effects on Elastics Constants of Technical Membranes Applying the Evaluation Methods of MSAJ/M-02-1995", *Membrane 2011 – 5th International Conference on Textile Composite and Inflatable Structures,* Barcelona, 2011.
[12] Cummings, R. M., Mason, W. H., Morton, S. A., Mcdaniel D. R., "Applied Computational Aerodynamics", Cambridge University Press, United States of America, 2015.
[13] Ormiston, R.A., "Theoritical and experimental aerodynamics of an elastic Sailwing", Dissertation, Princeton University, 1969.
[14] Mayle, R.E., "The Role of Laminar-Turbulent Transition in Gas Turbine Engines", *ASME Journal of Turbomachinery*, Vol. 113, pp. 509-537, 1991.
[15] Reuss Ramsay, R., Gregorek, G. M., "Effects of Grit Roughness and Pitch Oscillations on the S812 Airfoil", Airfoil Performance Report-NREL/SR-4408167, The Ohio State University, October 1998.